Article

Not peer-reviewed version

The Effect of Severe Plastic Deformation on the Microstructure and Mechanical Properties of Composite from 5056 and 1580 Aluminum Alloys Produced by Wire Arc Additive Manufacturing

Aydar Mavlyutov *, Alexey Evstifeev, Darya Volosevich, Marina Gushchina, Artem Voropaev, Oleg Zotov, Olga Klimova-Korsmik

Posted Date: 5 May 2023

doi: 10.20944/preprints202305.0367.v1

Keywords: wire arc additive manufacturing; microstructure; mechanical characteristics; aluminum-magnesium alloys; aluminum-scandium alloys; ultrafine-grained structure

Article

The Effect of Severe Plastic Deformation on the Microstructure and Mechanical Properties of Composite from 5056 and 1580 Aluminum Alloys Produced by Wire Arc Additive Manufacturing

Aydar Mavlyutov [1,2*], Alexey Evstifeev [1,3], Darya Volosevich [3], Marina Gushchina [1,3], Artem Voropaev [3], Oleg Zotov[4] and Olga Klimova-Korsmik [3]

[1] Saint Petersburg State University, Saint Petersburg, Russia
[2] Ioffe Institute, Saint Petersburg, Russia
[3] World-class Research Center, State Marine Technical University, Saint Petersburg, Russia
[4] Peter the Great Saint Petersburg Polytechnic University, Saint Petersburg, Russia
* Correspondence: aydarmavlyutov@mail.ioffe.ru

Abstract: In this study composite with alternate layers of 5056 and 1580 alloys was manufactured by wire arc additive manufacturing technology. It is shown that increased strength characteristics of composite material can be obtained due to deformation treatment by high-pressure torsion (HPT) technique. The microstructure and mechanical properties of the HPT-processed material in different structural states were investigated. The HPT-processed material exhibits high value of ultimate tensile strength (~ 770 MPa) but low ductility. Short-term annealing at 250 °C and additional deformation by HPT to 0.25 of revolution at room temperature resulted in a slight decrease in material's strength to ~ 700 MPa but provided ductility ~ 9%. Physical mechanisms to improve plasticity in correlation with microstructure evolution is discussed.

Keywords: wire arc additive manufacturing, microstructure, mechanical characteristics, aluminum-magnesium alloys, aluminum-scandium alloys, ultrafine-grained structure

1. Introduction

Material processing using wire arc additive manufacturing (WAAM) technologies makes it possible to obtain various products from a wide range of metallic materials. The technology makes it possible to manufacture component parts with high precision, unique geometry, and material variety layer by layer. The undeniable advantage of this technology is the reduction of cost and production time in piece production [1]. The WAAM technology could be a unique tool for creating new materials with given internal architecture that improves their mechanical and physical properties. It is well-known that severe plastic deformation (SPD) methods allow the formation of unique microstructure and properties in bulk metallic materials [2]. Various SPD methods have been developed and examined in recent years, the results of this investigations have been analyzed and summarized in recent reviews [2–6]. In recent years, many studies have been performed on SPD-processed pure aluminum and aluminum-based alloys [8–14]. It was shown that SPD processing results in formation ultrafine-grained structure providing high mechanical strength. Furthermore, in some cases, materials with enhanced mechanical strength demonstrate high ductility [13–14], although this is mutually exclusive properties for traditional metallic materials [15]. In [14] a new approach to improve plasticity while maintaining high strength of HPT processed commercially pure Al was proposed. This approach is based on the modification of the annealed structure of the high-angle grain boundaries by a slight additional deformation by HPT after short-term low-temperature annealing.

The Al-Mg alloys are the main material for the manufacture of space technology products, lightweight aluminum ships and various critical structures [16,17]. The hardening of the Al-Mg alloys

 doi:10.20944/preprints202305.0367.v1

is due to the formation of a solid solution, as well as through deformation treatment. As it was shown for equal-channel angular pressing (ECAP) processed Al–Mg alloys, increase in Mg content from 0.5 to 2 wt.% leads to grain grinding and increase in dislocation density [18]. The UFG Al–Mg alloys produced by high-pressure torsion (HPT) retained ductility at the acceptable level while Mg content is less than 2.5 wt.% [19]. Further increase in Mg content up to 4.1 wt.% results in decrease of ductility of HPT-processed alloy [20]. The increase of Mg content up to 4.5 wt.% completely suppresses plastic deformation in the HPT-processed material [19–20]. Thermal stability of nanostructured Al–Mg alloys remains unclear. One study found that Al–5Mg(wt.%) alloy treated by surface mechanical grinding has enhanced thermal stability of mechanical properties up to 200 °C [21]. Another study found degradation of mechanical properties of Al–5.5Mg(wt.%) alloy produced by ECAP with an increase in the annealing duration at 350 °C [22].

The problems mentioned above can be solved by introduction of alloying additives into the UFG Al-Mg alloy that increases strength and the recrystallization temperature. Among the alloying elements used in aluminum alloys, special attention is paid to Sc. It is one of the most effective modifiers, and even small Sc additives provide significant hardening and thermal stability [23–25].

In this work, an attempt to combine the WAAM and the SPD processes for creating of multi-layer aluminum materials has been made. In this framework, the 5056 Al-Mg and 1580 Al-Mg(Sc) alloys were chosen as a material for the investigation. The possibility of simultaneous increase in strength and ductility of the HPT-processed composite by additional deformation and heat treatment previously proposed in [14] was investigated.

2. Materials and Methods

The material for investigation were grown using a WAAM setup. The WAAM machine is based on the Fronius equipment package with cold material transfer technology. TPS 500i was used as a welding arc source. Fanuc M-710ic industrial robot was used as a moving system. Samples were deposited using high purity Ar shielding gas. Figure 1a shows a schematic representation of the deposition process. Deposition was carried out at 120 A, 14.8 V with travel speed 10–15 mm/s, the offset between adjacent beads was 3.2 mm. The composite sample were obtained by depositing alternating layers of 5056 and 1580 aluminum alloys stacked on top of each other, with thickness of each layer 2.5 mm until the following final dimensions of the sample: 30 mm in height, 30 mm in width and 100 mm in length. Schematic setup of the sample is shown on Figure 1b. The composite sample manufactured in this way is shown on Figure 2a. For HPT processing, disks with a diameter of 20 mm and a thickness of 1.5 mm were cut out from the sample according to the scheme (Figure 1b).

The HPT processing of the disks was performed on the Walter-Klement HPT press to 10 revolutions at room temperature (RT) under a pressure of 6 GPa. After HPT processing disks with a diameter of 20 mm and thickness of ~1.0 mm were formed. The logarithmic strain of material at the middle of the disk radius was $e \approx 5.5$ [26]. Additional deformation heat treatment included annealing at 200–275 °C for 1 h and further HPT processing to 0.25 revolutions at RT under the same pressure, which corresponded to the extra logarithmic strain of $e \approx 1.5$ [26].

Chemical analysis of the 5056 Al–Mg and 1580 Al-Mg(Sc) alloys and the HPT-processed sample was performed using the scanning electron microscope (SEM) equipped with an Energy Dispersive X-Ray (EDX) detector and the Oxford AZtec console (Oxford Instruments NanoAnalysis, United Kingdom).

Preprints (www.preprints.org) | NOT PEER-REVIEWED | Posted: 5 May 2023 doi:10.20944/preprints202305.0367.v1

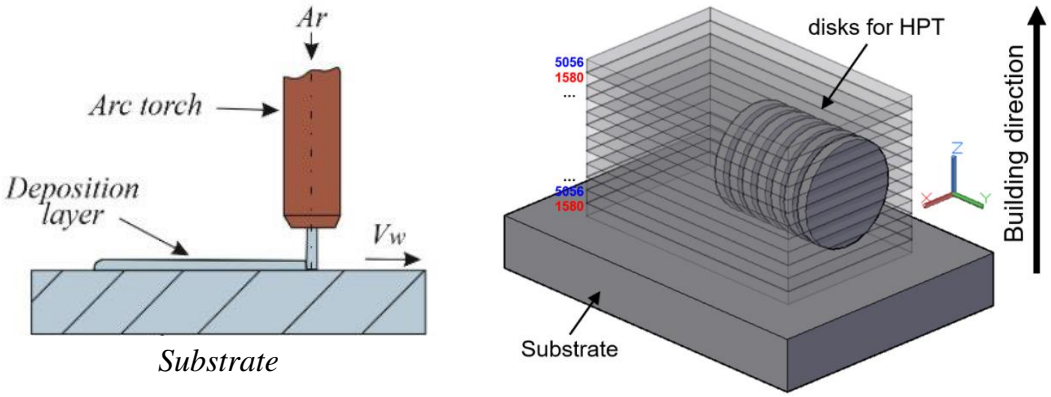

(**a**) (**b**)

Figure 2. Schematic representation of the deposition process (a); schematic setup of the sample obtained by depositing alternating layers of 1580 and 5056 aluminum alloys (b)

XRD analysis was performed on a Bruker D8 DISCOVER diffractometer in a symmetric θ–2θ scan modes using a parallel beam of CuKα radiation (40 kV, 40 mA). The scanning step was 0.02° and the time of exposure was 0.5 s. The average size of the coherent scattering regions (*C*) and the level of microdistortions of the crystal lattice ($\langle \varepsilon^2 \rangle^{1/2}$) were determined via the full-profile Pauli simulation using the TOPAS 5.0 software. The dislocation density was calculated according to the following ratio [27]:

$$L_{dis} = \frac{2\sqrt{3}\langle \varepsilon^2 \rangle^{1/2}}{Cb}, \quad (1)$$

where *b*=0.286 nm is the Burgers vector for edge dislocation in Al.

Transmission electron microscopy (TEM) was performed on an FEI Talos system equipped with a 200 kV field emission gun. Rapid TEM micrograph collection was undertaken at 25 frames per second, while collecting 512x512 pixel images. Samples for TEM studies were prepared using Mill TEM Model 1051 ion polishing machine.

Dog-bone samples with the gauge length of 6 mm and width of 2 mm were cut out from the disks according to the scheme (Figure 2b). The average values of the yield stress ($\sigma_{0.2}$) corresponding to 0.2% of deformation, the ultimate tensile strength (σ_{UTS}), the relative elongation to failure (δ), and the relative uniform elongation (δ_1) were determined by the tensile tests at a constant strain rate of 5 × 10^{-4} s^{-1}. Fracture surfaces of the destroyed samples were studied using the SEM Zeiss AURIGA at the accelerating voltage of 10 kV.

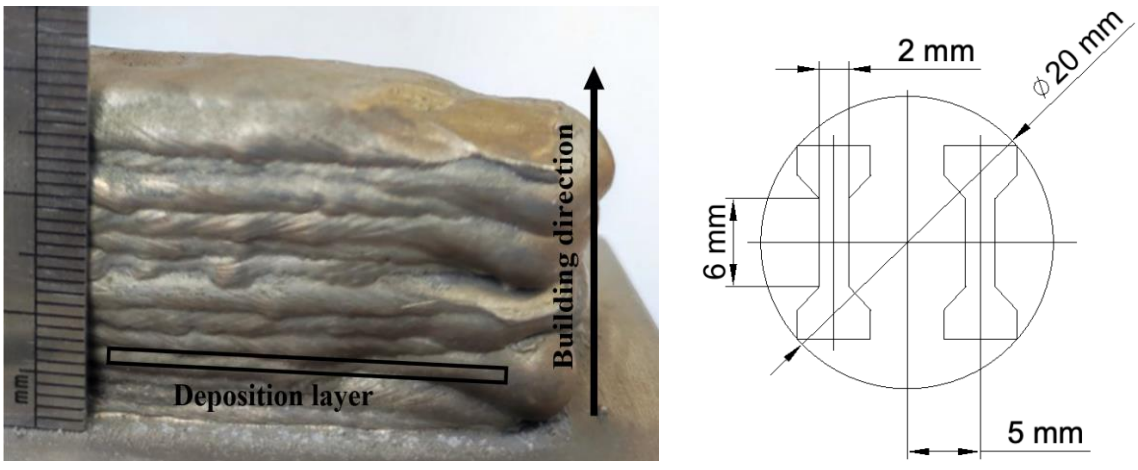

(**a**) (**b**)

Figure 2. Photo of the WAAM sample (a) and schematic representation of the dog-bone samples for mechanical tests (b)

Preprints (www.preprints.org) | NOT PEER-REVIEWED | Posted: 5 May 2023 doi:10.20944/preprints202305.0367.v1

3. Results and Discussion

Chemical composition (in wt. %) of the 5056 Al–Mg and 1580 Al-Mg(Sc) layers in the obtained by WAAM sample and the composite obtained by HPT is shown in Table 1. As can be seen, the concentration of Mg in the HPT-processed composite practically remains at the concentration level in 1580 alloy, but the concentration of Sc is significantly lower. The concentration of other elements is in the middle of concentration in two initial alloys.

Table 1. Chemical composition of 5056 Al-Mg, 1580 Al-Mg(Sc) alloys manufactured by WAAM method and the HPT-processed composite according to EDX analysis. The concentration is given in wt.%.

Material	Mg	Mn	Sc	Fe	Ti	Cr+V+Zn	Al
5056 alloy	4.94	0.14	-	0.09	0.14	<0.05	bal.
1580 alloy	4.61	0.55	0.08	0.17	0.1	<0.05	bal.
HPT-processed composite	4.66	0.27	0.03	0.11	0.12	<0.05	bal.

The stress-strain curves for the samples in different states of composite are shown on Figure 3. The initial state characterized by low tensile strength (σ_{UTS} ≈ 265 MPa) and high elongation to failure δ ≈ 21%. After HPT processing the ultimate strength of the material has tripled from ~ 265 to ~ 770 MPa, at the same time, samples demonstrated brittle behavior. Subsequent annealing of the HPT-processed material at 200–275 °C leads to even more embrittlement and the sample was destroyed at the external stress ~ 504 MPa (Table 2). After additional deformation by HPT to 0.25 revolutions the material demonstrates plasticity up to 10% (Figure 4). The best combination of tensile strength and plasticity was obtained after annealing at 250 °C and additional HPT to 0.25 revolutions. As a result, the yield stress ~ 590 MPa, ultimate tensile strength ~ 700 MPa, the uniform elongation ~3% and elongation to failure ~9% were obtained (Figure 4). The corresponding stress-strain curve is shown on (Figure 3). The results of the mechanical tests of the material in different structural states are summarized in Table 2.

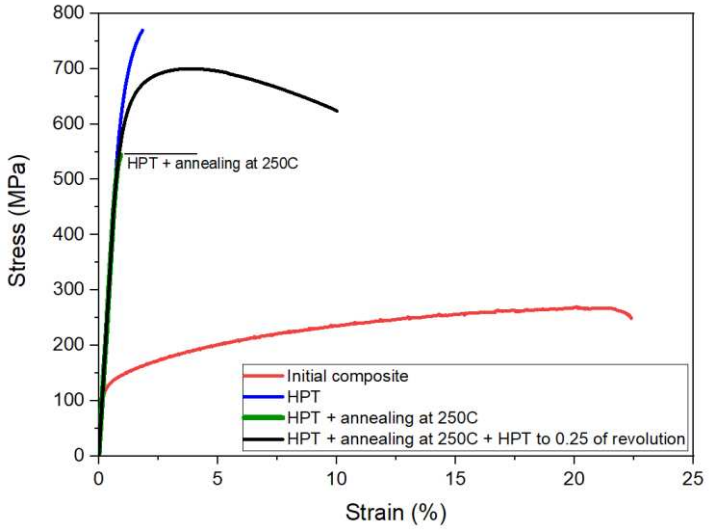

Figure 3. Stress-strain diagrams of composite in initial state, after HPT processing, after HPT processing and annealing at 250 °C for 1 h, after HPT processing, annealing at 250 °C for 1 h and additional HPT deformation to 0.25 revolutions.

Preprints (www.preprints.org) | NOT PEER-REVIEWED | Posted: 5 May 2023 doi:10.20944/preprints202305.0367.v1

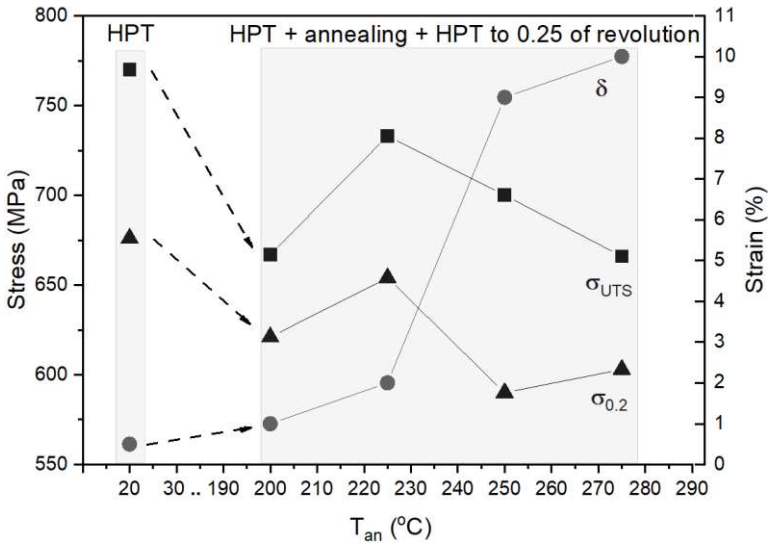

Figure 4. The dependences of ultimate tensile strength (σ_{UTS}), yield stress ($\sigma_{0.2}$), and elongation to failure (δ) on the annealing temperature for the composite samples, subjected to HPT, subsequent annealing and additional deformation by HPT to 0.25 of revolution.

Table 2. Mechanical properties of the composite in different structural states. $\sigma_{0.2}$ is the yield stress, corresponding to 0.2% of deformation, σ_{UTS} is the ultimate tensile strength, δ is the relative elongation to failure, δ_1 is the relative uniform elongation.

Composite material state	$\sigma_{0.2}$, MPa	σ_{UTS}, MPa	δ, %	δ_1, %
Initial composite	132±2	265±5	21±2	21±2
HPT	676±1	770±2	~0.5	~0.5
HPT + annealing at 200 °C	–	611±5	–	–
HPT + annealing at 250 °C	497±2	504±5	~0.2	~0.2
HPT + annealing at 200 °C + HPT to 0.25 of revolution	621±2	667±2	~1	~1
HPT + annealing at 225 °C + HPT to 0.25 of revolution	654±2	733±3	~2	~2
HPT + annealing at 250 °C + HPT to 0.25 of revolution	590±1	700±3	9±1	~3
HPT + annealing at 275 °C + HPT to 0.25 of revolution	603±2	666±3	10±1	~2

The fracture surface of samples after HPT, annealing at 250 °C and additional HPT processing is shown in Figure 5. The fracture surface of the HPT-processed material (Figure 5a,b) contains numerous micro- and macrocracks. Despite the severe destruction of the sample by a developed network of cracks, areas of plastic deformation still can be detected on the fracture surface (Figure 5,b) which indicates that the material has some plastic capacity, nonetheless uniform deformation do not exceed 1%. The fracture surface of sample after HPT processing and annealing at 250 °C is characterized by a brittle fracture with an extensive net of cracks along the surface of the working part of the sample (Figure 5c,d). There are no obvious traces of plastic deformation on the cracked surface. These results are fully correlate with X-ray analysis data showing the dislocation density reduction after annealing by an order of magnitude (Table 3). Additional HPT processing of the

Preprints (www.preprints.org) | NOT PEER-REVIEWED | Posted: 5 May 2023 doi:10.20944/preprints202305.0367.v1

annealed structure leads to the increase in dislocation density and the decrease in coherent scattering regions (Table 3). On the fracture surface (Figure 5e,f) it expressed by plastic deformation. The fracture surface is smoother and more homogeneous compared to the other structural states of the material.

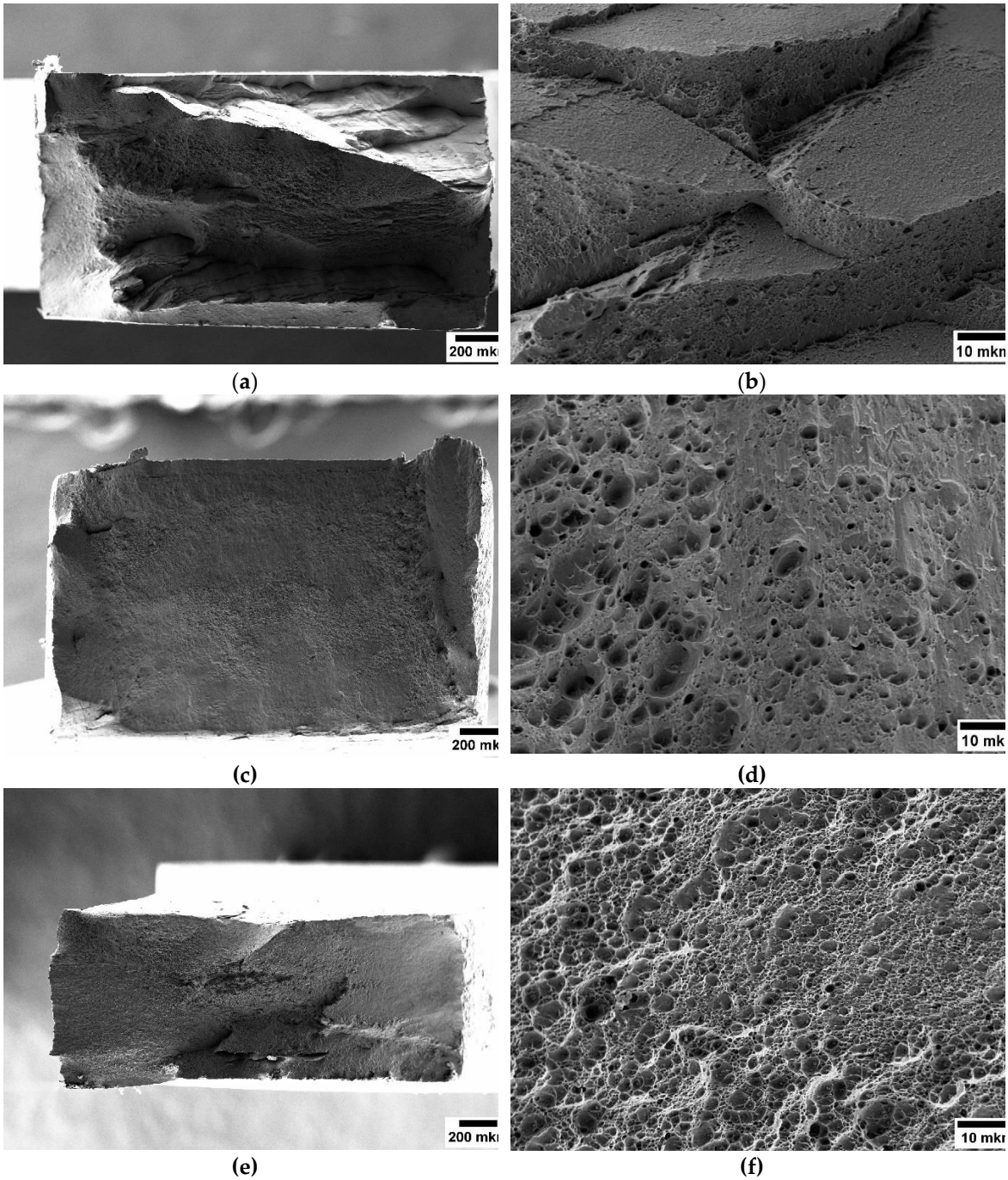

Figure 5. Fracture surface of the composite after HPT processing (a, b), after HPT processing and annealing at 250 °C for 1 h (c, d), after HPT processing, annealing at 250 °C for 1 h and additional HPT deformation to 0.25 revolutions (e, f).

Preprints (www.preprints.org) | NOT PEER-REVIEWED | Posted: 5 May 2023 doi:10.20944/preprints202305.0367.v1

Table 3. Microstructure parameters of the composite in different structural states. *C* is the size of coherent-scattering domains, $\langle\varepsilon^2\rangle^{1/2}$ is the elastic microdistortions level, L_{dis} is the dislocation density, d_{av} is the average grain size.

Composite material state	*C*, nm	$\langle\varepsilon^2\rangle^{1/2}$	$L_{dis}\cdot10^{13}$, m^{-2}	d_{av}, nm
HPT	300	0.0013	5.2	285
HPT + annealing at 250 °C	470	0.0002	0.4	330
HPT + annealing at 250 °C + HPT to 0.25 of revolution	200	0.0010	6.0	160

The TEM microstructure images of the composite in different structural states are shown in Figure 6. As it can be seen ultrafine-grained structure with uniaxial grains is formed upon HPT processing (Figure 6a). The average grain size determined on the basis of more than 100 measurements is $d_{av} \approx 285$ nm which correlates with the size of coherent-scattering domains obtained by XRD analysis (Table 3). Selected area electron diffraction pattern (the insert in Figure 6a) reveals the high-angle misorientation of grains. The grain size has a normal distribution which is shown on Figure 6b. After annealing at 250 °C, the average grain size and the distribution of grain size practically do not change (Figure 6c,d). However, the results of the mechanical tests indicate reduced yield stress and ultimate tensile strength (Table 2) after annealing. Such a drop in strength after annealing is typical for conventional coarse-grained metallic materials but usually accompanied by increased plasticity. The persistence of brittle behavior in our case may be associated with a decrease in the number of mobile dislocations during annealing as it was revealed by XRD analysis (Table 3). Additional deformation by HPT to 0.25 of revolution results in grain refinement up to ~160 nm (Figure 6e, Table 3). The grain size distribution remains normal (Figure 6d). According to the Hall-Petch ratio [28,29] such a grain refinement gives contribution to grain boundary strengthening $\Delta\sigma_{GB}\approx75$ MPa. Dislocation density increasing gives additional contribution to yield stress $\Delta\sigma_{dis}\approx40$ MPa caused by the action of dislocations strengthening mechanism [30]. These two mechanisms provide practically the same strengthening as the experimentally observed increase in yield stress $\Delta\sigma_{0.2} \approx 93$ MPa. One of the main explanations of manifestation of plastic properties after additional HPT processing can be given on the bases of the model proposed earlier in [31]. After additional deformation by HPT the deformation-induced dislocations are formed in a dislocation pile-ups in triple junctions of high-angle grain boundaries, increased plasticity occurs through the emission of lattice dislocations from triple junctions of grain boundaries, the glide of the lattice dislocations across neighboring grains, their accumulation at and climb along the opposite grain boundaries.

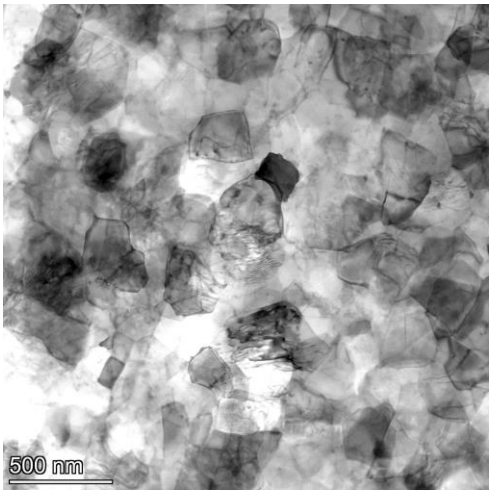

(**a**)

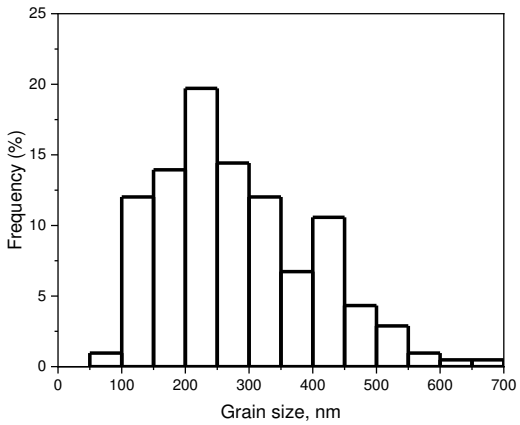

(**b**)

Preprints (www.preprints.org) | NOT PEER-REVIEWED | Posted: 5 May 2023 doi:10.20944/preprints202305.0367.v1

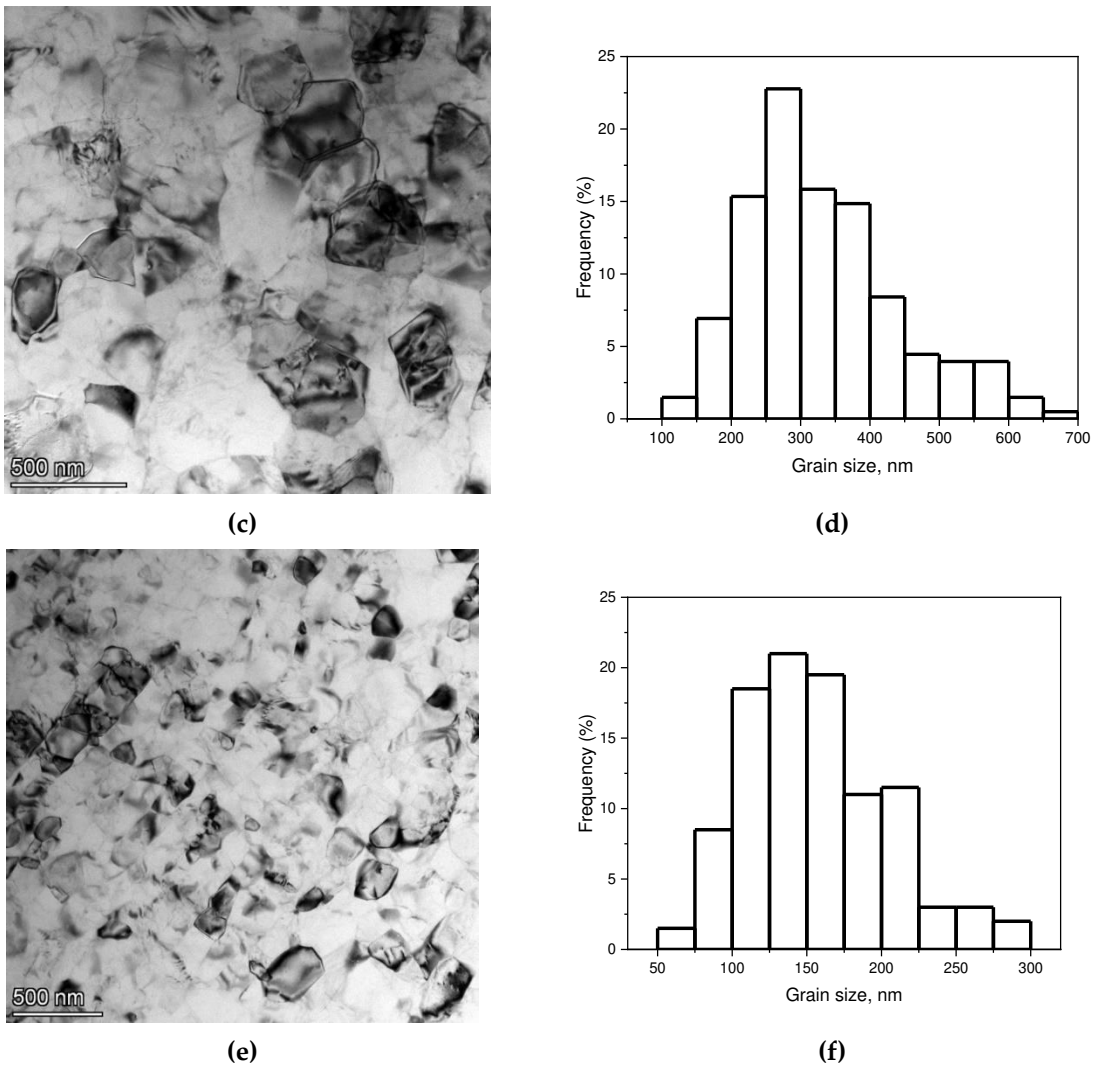

Figure 6. TEM micrographs of the composite after HPT processing (a), subsequent annealing at 250 °C (c) and addition deformation by HPT to 0.25 of revolution (e) and corresponding grain size distribution (b), (d) and (f).

5. Conclusions

The results show the potential of combination wire arc additive manufacturing and high-pressure torsion technique for producing composite materials with high mechanical characteristics. The ultimate strength of the HPT-processed composite material can reach ~770 MPa. It's by ~ 3 times more than initial strength properties. However, the material exhibits low ductility, which is a limitation for many practical applications. It was found that deformation-heat treatment comprising short-term annealing at 250 °C and additional deformation by HPT to 0.25 of revolution at room temperature is an effective way to improve the ductility of the material while maintaining a high level of strength. The resulting material had a tensile strength of ~700 MPa, which was still 90% of the strength value after HPT processing, with a significant increase in ductility to approximately 9%.

The combination of sufficient ductility and high tensile strength was obtained by introducing of an additional dislocation density into the grain boundary or near grain boundary structure. The proposed approach suggests high potential for practical applications of the alloy studied and can be a universally effective way to achieve a combination of high strength and ductility for various UFG materials.

Author Contributions: A.M.: conceptualization, methodology, validation, analysis, supervision, writing—original draft, writing—review and editing. A.E.: investigation, data curation, visualization, XRD analysis and writing—original draft. D.V.: SEM and EDX analysis. M.G.: TEM analysis and editing. A.V.: participation in

experimental work and visualization. O.Z.: participation in analysis and visualization. O.K.: conceptualization, analysis and writing—review and editing. All authors have read and agreed to the published version of the manuscript.

Funding: This research was funded by Russian Science Foundation, grant number 22-79-10043. WAAM printing technology was implemented as part of the World-class Research Center program: Advanced Digital Technologies (Contract no. 075-15-2022-312 dated 20 April 2022).

Data Availability Statement: The data presented in this study are available on request from the corresponding author.

Acknowledgments: The mechanical and structural studies were performed using the equipment of the Laboratory for Mechanics of Advanced Bulk Nanomaterials for Innovative Engineering Applications of St. Petersburg State University and the "Interdisciplinary Resource Center for Nanotechnology" and the "Centre for X-ray Diffraction Studies" of the Research Park of St. Petersburg State University.

Conflicts of Interest: The authors declare no conflict of interest.

References

1. Ding, J.; Baumers, M.; Clark, E.A.; Wildman, R.D. The economics of additive manufacturing: Towards a general cost model including process failure. *Int. J. Production Economics* **2021**, *237*, 108087. DOI: 10.1016/j.ijpe.2021.108087
2. Zhu, Y.; Valiev, R.Z.; Langdon, T.G.; Tsuji, N.; Lu, K. Processing of nanostructured metals and alloys via plastic deformation. *MRS Bulletin* **2010**, *35*, 977–981. DOI: 10.1557/mrs2010.702
3. Estrin, Y.; Vinogradov, A. Extreme grain refinement by severe plastic deformation: A wealth of challenging science. *Acta Mater.* **2013**, *61*, 782–817. DOI: 10.1016/j.actamat.2012.10.038
4. Langdon, T.G. Twenty-five years of ultrafine-grained materials: Achieving exceptional properties through grain refinement. *Acta Mater.* **2013**, *61*, 7035–7059. DOI: 10.1016/j.actamat.2013.08.018
5. Sabirov, I.; Murashkin, M.Yu.; Valiev, R.Z. *MSEA* **2013**, *560*, 1–24. DOI: 10.1016/j.msea.2012.09.020
6. Kawasaki, M.; Langdon, T.G. Review: achieving superplasticity in metals processed by high-pressure torsion. *J. Mater. Sci.* **2014**, *49*, 6487–6496. DOI: 10.1007/s10853-014-8204-5
7. Duchaussoy, A.; Sauvage, X.; Edalati, K.; Horita, Z.; Renou, G.; Deschamps, A.; De Geuser, F. Structure and mechanical behavior of ultrafine-grained aluminum-iron alloy stabilized by nanoscaled intermetallic particles. *Acta Mater.* **2019**, *167*, 89–102. DOI: 10.1016/j.actamat.2019.01.027
8. Talebanpour, B.; Ebrahimi, R.; Janghorban, K. Microstructural and mechanical properties of commercially pure aluminum subjected to dual equal channel lateral extrusion. *MSEA* **2009**, *527*, 141–145. DOI: 10.1016/j.msea.2009.07.040
9. Sabirov, I.; Murashkin, M.Yu.; Valiev, R.Z. Nanostructured aluminium alloys produced by severe plastic deformation: New horizons in development. *MSEA* **2013**, *560*: 1–24. DOI: 10.1016/j.msea.2012.09.020
10. Mavlyutov, A.M.; Bondarenko, A.S.; Murashkin, M.Y.; Boltynjuk, E.V.; Valiev, R.Z.; Orlova, T.S. Effect of annealing on microhardness and electrical resistivity of nanostructured SPD aluminium. *Jour. Alloys Comp.* **2017**, *698*, 539–546. DOI: 10.1016/j.jallcom.2016.12.240
11. Mavlyutov, A.M.; Kasatkin, I.A.; Murashkin, M.Yu.; Valiev, R.Z.; Orlova, T.S. Influence of the microstructure on the physicomechanical properties of the aluminum alloy Al–Mg–Si nanostructured under severe plastic deformation. *Phys. Solid State* **2015**, *57*, 2051–2058. DOI: 10.1134/S1063783415100194
12. Huang, X.; Hansen, N.; Tsuji, N. Hardening by annealing and softening by deformation in nanostructured metals. *Science* **2006**, *312*, 249–251. DOI: 10.1126/science.1124268
13. Kamikawa, N.; Huang, X.; Tsuji, N.; Hansen, N. Strengthening mechanisms in nanostructured high-purity aluminium deformed to high strain and annealed. *Acta Mater.* **2009**, *57*, 4198–4208. DOI: 10.1016/j.actamat.2009.05.017.
14. Mavlyutov, A.M.; Latynina, T.A.; Murashkin, M.Yu.; Valiev, R.Z.; Orlova, T.S. Effect of annealing on the microstructure and mechanical properties of ultrafine-grained commercially pure Al. *Phys. Solid State.* **2017**, *59*, 1970–1977. DOI: 10.1134/S1063783417100274
15. Valiev, R.Z.; Alexandrov, I.V.; Zhu, Y.T.; Lowe, T.C. Paradox of Strength and Ductility in Metals Processed by Severe Plastic Deformation. *Jour. Mater. Res.* **2002**, *17*, 5–8. DOI: 10.1557/JMR.2002.0002
16. Mondolfo, L.F. Aluminum alloys: structure and properties. Elsevier, 2013.
17. Aluminum Association. Aluminum: properties and physical metallurgy. ASM International, 1984.

18. Kalsar, R.; Yadav, D.; Sharma, A.; Brokmeier, H.G.; May, J.; Höppel, H.W.; Skrotzki, W.; Suwas, S. Effect of Mg content on microstructure, texture and strength of severely equal channel angular pressed aluminium-magnesium alloys. *MSEA* **2020**, 797, 140088. DOI: 10.1016/j.msea.2020.140088
19. Liu, M.P.; Roven, H.J.; Murashkin, M.Yu.; Valiev, R.Z.; Kilmametov, A.; Zhang, Z.; Yu, Y. Structure and mechanical properties of nanostructured Al-Mg alloys processed by severe plastic deformation. *J. Mater. Sci.* **2013**, *48*, 4681–4688. DOI:10.1007/s10853-012-7133-4
20. Liu, Y.; Liu, M.; Chen, X.; Cao, Y.; Roven, H.J.; Murashkin, M.; Zhou, H. Effect of Mg on microstructure and mechanical properties of Al-Mg alloys produced by high pressure torsion. *Scr. Mater.* **2019**, *159*, 137–141. DOI: 10.1016/j.scriptamat.2018.09.033.
21. Xu, W.; Zhang, B.; Du, K.; Li, X.Y.; Lu, K. Thermally stable nanostructured Al-Mg alloy with relaxed grain boundaries. *Acta Mater.* **2022**, *226*, 117640. DOI: 10.1016/j.actamat.2022.117640
22. Snopiński, P.; Tański, T. Thermal stability and microstructure evolution of ultra-fine grained Al-Mg alloy. IOP Conference Series: *Mater. Sci. Eng.* **2018**, *461*, 012085. DOI: 10.1088/1757-899X/461/1/012085
23. Konstantinov, I.L., Baranov, V.N., Sidelnikov, S.B.; Kulikov, B.P.; Bezrukikh, A.I.; Frolov, V.F.; Orelkina, T.A.; Voroshilov, D.S.; Yuryev, P.O.; Belokonova, I.N. Investigation of the structure and properties of cold-rolled strips from experimental alloy 1580 with a reduced scandium content. *Int. J. Adv. Manuf. Technol.* **2020**, *109*, 443–450. DOI:10.1007/s00170-020-05681-4
24. Konstantinov, I.L.; Baranov, V.N.; Sidelnikov, S.B.; Zenkin, E.Y.; Yuryev, P.O.; Belokonova, I.N. Influence of Rolling and Annealing Modes on Properties of Sheet Semifinished Products Made of Wrought Aluminum Alloy 1580. *Russ. J. Non-ferrous Metals* **2020**, *61*, 641–645. DOI: 10.3103/S1067821220060115
25. Johansen, A. *Microstructures and properties of aluminium-magnesium alloys with additions of manganese, zirconium and scandium.* Trondheim: Norwegian University of Science and Technology 2000. 230 p.
26. Zhilyaev, A.P.; Langdon, T.G. Using high-pressure torsion for metal processing: Fundamentals and applications. *Prog. Mater. Sci.* **2008**, *53*, 893–979. DOI: 10.1016/j.pmatsci.2008.03.002
27. Williamson, G.K.; Smallman, R.E. III. Dislocation densities in some annealed and cold-worked metals from measurements on the X-ray debye-scherrer spectrum. *Philos. Mag.* **1956**, *1*, 34–46. DOI:10.1080/14786435608238074
28. Hall, E.O. The Deformation and Ageing of Mild Steel: III Discussion of Results. *Proc. Phys. Soc. B* **1951**, *64*, 747. DOI:10.1088/0370-1301/64/9/303
29. Petch, N.J. The orientation relationships between cementite and α-iron. *Acta Cryst.* **1953**, *6*, 96–96. DOI: 10.1107/S0365110X53000260
30. Hansen, N.; Huang, X. Microstructure and flow stress of polycrystals and single crystals. *Acta Mater.* **1998**, *46*, 1827–1836. DOI:10.1016/S1359-6454(97)00365-0
31. Orlova, T.S.; Skiba, N.V.; Mavlyutov, A.M.; Murashkin, M.Y.; Valiev, R.Z.; Gutkin, M.Y. Hardening by annealing and implementation of high ductility of ultra-fine grained aluminum: experiment and theory. *Rev. Adv. Mater. Sci.* **2018**, *57*, 224–240. DOI: 10.1515/rams-2018-0068